REPORT DOCUMENTATION PAGE

Form Approved OMB NO. 0704-0188

1. REPORT DATE (DD-MM-YYYY)	2. REPORT TYPE	3. DATES COVERED (From - To)
14-09-2023	Final Report	15-Jun-2020 - 14-Jun-2023

4. TITLE AND SUBTITLE
Final Report: Optically-driven optical isolation and magnetism in an integrated photonic platform

5a. CONTRACT NUMBER
W911NF-20-1-0217

5b. GRANT NUMBER

5c. PROGRAM ELEMENT NUMBER
611102

6. AUTHORS

5d. PROJECT NUMBER

5e. TASK NUMBER

5f. WORK UNIT NUMBER

7. PERFORMING ORGANIZATION NAMES AND ADDRESSES
University of Chicago
5801 South Ellis Avenue
Chicago, IL 60637 -5418

8. PERFORMING ORGANIZATION REPORT NUMBER

9. SPONSORING/MONITORING AGENCY NAME(S) AND ADDRESS (ES)
U.S. Army Research Office
P.O. Box 12211
Research Triangle Park, NC 27709-2211

10. SPONSOR/MONITOR'S ACRONYM(S)
ARO

11. SPONSOR/MONITOR'S REPORT NUMBER(S)
76832-ES.11

12. DISTRIBUTION AVAILIBILITY STATEMENT
Approved for public release; distribution is unlimited

13. SUPPLEMENTARY NOTES
The views, opinions and/or findings contained in this report are those of the author(s) and should not contrued as an official Department of the Army position, policy or decision, unless so designated by other documentation.

14. ABSTRACT

15. SUBJECT TERMS

16. SECURITY CLASSIFICATION OF:			17. LIMITATION OF ABSTRACT	15. NUMBER OF PAGES	19a. NAME OF RESPONSIBLE PERSON
a. REPORT	b. ABSTRACT	c. THIS PAGE			Alexander High
UU	UU	UU	UU		19b. TELEPHONE NUMBER 773-834-0932

RPPR Final Report
as of 18-Sep-2023

Agency Code: 21XD

Proposal Number: 76832ES **Agreement Number: W911NF-20-1-0217**
INVESTIGATOR(S):

Name: Alexander A. High
Email: ahigh@uchicago.edu
Phone Number: 7738340932
Principal: Y

Organization: **University of Chicago**
Address: 5801 South Ellis Avenue, Chicago, IL 606375418
Country: USA
DUNS Number: 005421136 EIN: 362177139
Report Date: 14-Sep-2023 Date Received: 14-Sep-2023
Final Report for Period Beginning 15-Jun-2020 and Ending 14-Jun-2023
Title: Optically-driven optical isolation and magnetism in an integrated photonic platform
Begin Performance Period: 15-Jun-2020 **End Performance Period:** 14-Jun-2023
Report Term: 0-Other
Submitted By: Alexander High Email: ahigh@uchicago.edu
Phone: (773) 834-0932

Distribution Statement:

STEM Degrees: 2 **STEM Participants:** 3

Major Goals: In this research proposal, we investigated new device architectures that will enable optically-driven, on-chip nanophotonic isolators with micron-scale footprints and low power requirements for control. The continued evolution of integrated photonics demands increasingly compact, power efficient devices that provide sophisticated functionalities for next generation applications. Common needs appearing across several fields include all-optical control, optical memory, and non-reciprocity. For instance, the emerging field of photonic neuromorphic computing relies on integrated optical memories as photonic synapses for self-tailored signal transmission through neural networks. In integrated LIDAR and photonic circuits, isolation is vital to protect light sources and prevent crosstalk. In topological photonics, breaking time-reversal symmetry through magnetic biasing or complex temporal modulation is required for robust edge state protection. By using optical drives and micron-scale photonics structures instead of magnets and millimeter-scale photonic structures, we can significantly improve the integration of these devices. Our methodology relies on optical spin-orbit coupling (OSOC) in nanophotonic structures coupled to 2D materials as a mechanism to break time-reversal symmetry and enable isolation. While, there are other actively-investigated approaches to generating non-reciprocity in photonics without magnetic fields, such as topological photonics, balanced gain-loss systems, electro-optic modulators, and coupled non-near oscillators, we our approach is intrinsically simple and compact, and utilizes micron-scale ring- and disk-resonators and linear driving fields to create new technologies.

The first goal of this research is to leverage optical spin-orbit coupling (OSOC) in photonic structures to optically-drive magnetic phenomena in semiconducting transition metal dichalcogenides (TMDs) and in turn generate on-chip isolation. TMDs host optical exciton transitions with exceptionally large oscillator strengths and valley-dependent circular polarization. We are able to create intense, circularly-polarized optical fields in photonic ring resonators with moderate input powers. In direct proximity to the resonator, TMDs will interact with the chiral fields. One interaction mechanism is the valley-dependent optical Stark effect (OSE). We have performed a full numerical analysis of this interaction that combines simulations of optical fields and experimentally-measured quality factors of photonic cavities with known material properties of TMDs. We calculate that we can optically-drive energetic spin splitting of exciton transitions in TMDs of 16 meV or greater - equivalent to placing the material in a 100 Tesla magnetic field. This interaction breaks time-reversal symmetry in the TMD, and enables all-optical on-chip isolation in integrated photonics, with predicted isolation of greater than 35 dB. We recently uncovered an additional interaction mechanism that can be leveraged for generating isolation. We have observed that we can optically drive magnetism in electrons in 2D materials with microwatt level optical pumps (this is also discussed in the secondary objective below). This magnetism creates a large circular dichroism in the material – indeed, the excitonic resonances can be up to %90 circularly polarized. While we are still in the initial phase of this discovery, this large

dichroism can be applied to isolation, and we are eagerly exploring this avenue in the next phase of research.

The second goal of this research proposal is to determine if OSOC in integrated photonics can optically control magnetic solid-state memories. Specifically, we will determine if OSOC can control spin magnetism in electronically-doped TMDs. This research can break new ground in our ability to control spins in solid-state materials. If successful, the same techniques can be applied directly to more commonly utilized magnetic thin films. Such control would advance optical computing and interconnects by creating a new photonic interface with traditional solid state electronic computing. Beyond improved integration possibilities, optically driven magnetism offers additional advantages over traditional magnetic systems, including to the capability to be reconfigured at ultra-fast timescales, enabling dynamic control, and memory control without energy consuming electronics. Additionally, the magnetic state can also exhibit strong circular dichroism. This can be additionally leveraged for isolation.
Our accomplishments will be discussed in depth in the following section, but here we briefly describe the proposed research timeline and completion percentage. The completion percentage will also be discussed in depth in the accomplishments section.
Towards goal 1, we set the following targets: Target 1 (75% completed) for years 1 and 2: Generation and Mapping of the optical Stark Effect. Target 2 (50% completed) for years 2-3: Generation of optical isolation. Target 3 (50% completed) for year 3: Optimization of isolation and exploration of broader wavelength regimes
Towards goal 2, we set the following targets: Target 1 (100% completed) for Years 2 and 3: Optical control and mapping of spin populations. Target 2 (100% completed) fo year 3: Dynamic control of spin and magnetism.

Accomplishments: The first goal of this research is to leverage optical spin orbit coupling (OSOC) in photonic structures to optically drive magnetic phenomena in semiconducting transition metal dichalcogenide monolayers (TMDCs) and igenerate on-chip isolation. OSOC is a phenomena in which the microscopic optical fields of photonic resonators and waveguides can exhibit near-perfect circular polarization in which the helicity is locked to propagation direction. This feature of tightly confined light allows propagation-direction-dependent interactions with optical materials, yielding chiral light-matter interfaces with applications including unidirectional photon routing and optical isolation.

We pursued a multi-phase research effort to realize such coupling with TMDCs. First, we established and verify a chiral nanophotonic interface with TMDCs, in which the excitonic states exhibit helicity- dependent directional-coupling to integrated photonic structures. Through a combination of simulation-based design, fabrication optimization, and enhanced measurement capability, we succeeded in creating this chiral interface, and added additional tunability beyond the initial aims of the proposal. This research was reported in our manuscript "Electrically controllable chirality in a nanophotonic interface with a two-dimensional semiconductor", published in Nature Photonics. We can now fabricate TiO2 waveguides directly on the surface of low-disorder, boron-nitride-encapsulated WSe2 with no observable impact to material quality. We demonstrated that we can dynamically switch the optical coupling of the 2D semiconductor and a photonic waveguide between a chiral, directionally biased state and a non-chiral, balanced state. Our development leverages the gate-tunable valley polarization of excitonic states in 2D semiconductors and our newly developed capability to integrate nanophotonics with van der Waals heterostructures. Beyond active control of chirality, our work demonstrated multiple noteworthy advancements. First, the photonic fabrication method provides a general platform for on-demand patterning of photonic structures on 2D materials with no deleterious impacts to material quality. This procedure will have an impact on interfacing scalable photonic devices with van der Waals heterostructures and wafer-scale monolayers. Second, near-field excitation through the photonic waveguide generates directionally reconfigurable, valley(spin)-polarized exciton fluxes. Our versatile fabrication approach enables deterministic integration of photonics with low-disorder van der Waals heterostructures and opens new pathways towards optically driving chiral excitonic and charge-carrier phenomena therein. Additionally, over the three years of the project, we continued to refine our fabrication of ring resonators and photonic devices integrated into van der Waals heterostructures and build more in-depth knowledge of the tunable optical response of 2D materials. This work has set the stage for follow up research supported by the ARO.

The second goal of the proposal is to determine if OSOC in integrated photonics can optically-control magnetic solid-state memories. Such control would advance optical computing and interconnects by creating a new photonic interface with traditional solid state electronic computing. Over the three years of ARO-sponsored research, we made significant progress and were able to fully achieve these goals.

We discovered mesoscopic, optically controllable ferromagnetic order exists in monolayer TMDCs – specifically in encapsulated monolayer tungsten diselenide (WSe2). Remarkably, we have also demonstrated that such magnetic

order is fully controlled by local optical pumps, even in the absence of magnetic fields. We reported these observations in our manuscript "Optically Controllable Magnetism in Atomically Thin Semiconductors", published in Science Advances. In these experiments, we utilize electronic doping to tune the carrier density in WSe2 into a regime that favors formation of magnetic order. We then demonstrated that a circularly-polarized, microwatt-power, diffraction-limited optical pump is sufficient to break symmetry and generate a single magnetic phase that extends over an area of 40 μm2. The experimental signature of the magnetic order is circular dichroism in reflectivity, which reaches values greater that 20% and corresponds to an electronic spin and valley polarization of 90%. The orientation of the magnetic state is dictated by the helicity of the pump. In comparison to previous studies of magnetism in 2D materials that require global, weakly tunable external magnetic fields to manipulate magnetic phases, our method enables complete control over magnetism with local, highly tunable optical fields. We also demonstrated that our integrated photonic waveguides can effectively control the magnetic state of the electrons, again confirming the chiral interface developed in goal 1 of the proposal. Additionally, we demonstrated an entirely new phenomenon, spin amplification, in which the interactions between electrons actually inc. In particular, we were able to show that the peak spin polarization observed at a spatial separation of 3 microns exceeded the predictions of a diffusion model by a factor of 40. Spin amplification can enable low-power control of electron memories and fan-out in spin-tronic devices.
This research has effectively bridged two of the most exciting areas in 2D materials research – correlated electronic phases at low carrier densities and magnetism – and created a versatile method to optically manipulate these systems. In addition, the capability to optically manipulate magnetic memory and corresponding circular dichroism in TMDCs will stimulate new developments in optoelectronics and spintronics. We have submitted a patent application for the process to control magnetism. The huge circular dichroism that accompanies the magnetic phase will directly enable the development of isolators and other all-optical logic that seamlessly integrates with a solid state memory, which we will explore in the next phase of research.
Stated goals not met: We were unable to fully realize our first goal of generating optical isolation in integrated photonics by utilizing the AC Stark effect. This was due to issues coupling the ~10 milliwatts of control power into the photonic cavities - we were unable to hit the coupling efficiency of ~15% predicted in our simulations. We also observed broader-than-expected absorption in our photonic cavities near the exciton resonances in TMDs. While this confirmed interaction between the waveguided light and the TMD, it also diminished the quality factors of our cavities. However, we did significantly improve our photonics integration with 2D materials and fully verify the chiral photonic properties of the photonic interface with the 2D materials. In the next phase of research, we are exploring optical control methods that require microwatt level inputs (orders of magnitude lower than in the original proposal and easily realized in our coupling scheme) and that will allow us to work at wavelengths farther away from the absorptive exciton wavelengths. Therefore, we give an approximate completion percentage for the targets of the first research thrust ranging from %50-75%.

Training Opportunities: PI High has supervised several students and a postdoctoral fellow that were involved in the sponsored research. All students and postdocs received direct one-on-one mentorship and had the opportunity to present their research at conferences, described in the dissemination section. The ARO funds provided support for two PhD students in my lab, Robert Shreiner (75% support over the last year) and Andrew Kindseth (25% support over the last year). Robert earned his PhD in April of 2023. The ARO funding was used to pay graduate stipend, tuition, and other fees related to graduate school. Over the course of the last year, Robert and Andrew gained significant training in the usage of sophisticated cleanroom equipment, which can transfer to future careers in technology and engineering. Additionally, they developed new experimental methods in the lab, under my supervision.
ARO funding was also used to support Postdocotral fellow Kai Hao (25% over the last year). Kai is currently applying to faculty positions in the United States and has had several interviews so far.
University of Chicago undergraduate student Christopher Cheung participated in the research on optically controllable magnetism. He graduated in Spring of 2023 and is now beginning his PhD at Princeton University.

RPPR Final Report
as of 18-Sep-2023

Results Dissemination: Manuscripts: Research supported by ARO funding was reported in two published manuscripts: (1) "Electrically controllable chirality in a nanophotonic interface with a two-dimensional semiconductor" published in Nature Photonics, https://www.nature.com/articles/s41566-022-00971-7 (2) "Optically controllable magnetism in atomically thin semiconductors," published in Science Advances, https://www.science.org/doi/10.1126/sciadv.abq7650. (3) "Robotic four-dimensional pixel assembly of van der Waals solids", published in Nature Nanotechnology, https://www.nature.com/articles/s41565-021-01061-5. The manuscripts have collectively been accessed 30000 times according to the article metrics. Additionally, the research was covered in an additional News and Views article "Chiral quantum optics goes electric", published in Nature Photonics https://www.nature.com/articles/s41566-022-00982-4. The News and Views is targeted to the general public.

Conference presentations and invited talks: PI High gave the following invited presentations on the research: (1) Brockhouse Institute for Materials Research Workshop on Future Materials June 1, 2023 (2) SPIE Photonics West February 2, 2023 (3) Tholous Institute for Quantum Matter, University of Washington, April 14, 2022
Graduate Student Robert Shreiner gave contributed presentations at the 2022 APS March Meeting and 2023 APS March Meeting on the funded research.
Postdoctoral Fellow Kai Hao gave contributed presentations at the 2022 APS March Meeting and 2023 APS March Meeting on the funded research.
Graduate Student Andrew Kindseth participated in a poster session at the 2023 APS March Meeting

Dissemination in other media: In parallel with our publication in Nature Photonics, we worked with university of chicago to create a press release, https://pme.uchicago.edu/news/ultra-compact-integrated-photonic-device-could-lead-new-optical-technologies, that was broadly disseminated. As a result of the press release, PI High appeared on the official podcast of Electronic Engineering Journal, the Fish Fry podcast, https://www.eejournal.com/fish_fry/guiding-light-university-of-chicago-research-team-develops-a-whole-new-class-of-integrated-photonic-circuits/

Honors and Awards: Nothing to Report

Protocol Activity Status:

Technology Transfer: “Optically controllable mesoscopic magnetism in semiconductors”, United States Patent Application 63/231,817, Filed August 11, 2021

PARTICIPANTS:

Participant Type: PD/PI
Participant: Alexander Arthur High
Person Months Worked: 1.00 **Funding Support:**
Project Contribution:
National Academy Member: N

Participant Type: Graduate Student (research assistant)
Participant: Robert Shreiner
Person Months Worked: 9.00 **Funding Support:**
Project Contribution:
National Academy Member: N

Participant Type: Graduate Student (research assistant)
Participant: Andrew Kindseth
Person Months Worked: 3.00 **Funding Support:**
Project Contribution:
National Academy Member: N

RPPR Final Report
as of 18-Sep-2023

Participant Type: Postdoctoral (scholar, fellow or other postdoctoral position)
Participant: Kai Hao
Person Months Worked: 3.00 **Funding Support:**
Project Contribution:
National Academy Member: N

Participant Type: Undergraduate Student
Participant: Christopher Cheung
Person Months Worked: 3.00 **Funding Support:**
Project Contribution:
National Academy Member: N

ARTICLES:

Publication Type: Journal Article Peer Reviewed: Y **Publication Status:** 1-Published
Journal: Science Advances
Publication Identifier Type: DOI Publication Identifier: 10.1126/sciadv.abq7650
Volume: 8 Issue: 39 First Page #: eabq7650
Date Submitted: 9/11/23 12:00AM Date Published:
Publication Location: Washington DC
Article Title: Optically controllable magnetism in atomically thin semiconductors
Authors: Kai Hao, Robert Shreiner, Andrew Kindseth, Alexander A. High
Keywords: magnetism, 2D materials, dichroism, optical control
Abstract: We report evidence that ferromagnetic order in electrostatically-doped, monolayer transition metal dichalcogenide (TMD) semiconductors can be stabilized and controlled at zero magnetic field by local optical pumping. We use circular dichroism (CD) in reflectivity from excitonic states as a spatially-resolved probe of charge-carrier spin polarization. At electron densities ne ~ 1012 cm-2, a diffraction-limited, circularly-polarized optical pump breaks symmetry between oppositely-polarized magnetic states and stabilizes long-range magnetic order, with carrier polarization exceeding 80% over an 8 μm by 5 μm extent. In time-resolved measurements with pulsed optical excitation, we observe that magnetic interactions amplify the initial pump-induced spin polarization by more than an order of magnitude. The optical control of magnetism with local optical pumps will unlock new spin and optical technologies and provide a versatile tool in the study of correlated phases.
Distribution Statement: 1-Approved for public release; distribution is unlimited.
Acknowledged Federal Support: **Y**

RPPR Final Report
as of 18-Sep-2023

Publication Type: Journal Article Peer Reviewed: Y **Publication Status:** 5-Submitted
Journal: under consideration at Nature Photonics
Publication Identifier Type: Publication Identifier:
Volume: Issue: First Page #:
Date Submitted: 8/24/21 12:00AM Date Published:
Publication Location:
Article Title: Electrically controllable chirality in a nanophotonic interface with a 2D semiconductor
Authors: Robert Shreiner, Kai Hao, Amy Butcher, Alexander High
Keywords: integrated photonics, chiral interface, electric tunability
Abstract: Subwavelength control of optical fields in nanophotonic structures creates new opportunities for engineering light-matter interactions. Notably, waveguided optical modes display circularly polarized evanescent fields with wavevector-dependent, transverse spin angular momentum1-3. This feature of tightly confined light – termed optical spin-orbit coupling – allows propagation direction-dependent interactions with optical materials4-6, yielding chiral light-matter interfaces with applications including unidirectional photon routing7,8 and optical isolation9,10. Electrical tuning of interface chirality would enable active, switchable non-reciprocity in on-chip optoelectronic and photonic circuitry, but remains an outstanding challenge. Here, we report electrically controllable chirality in a nanophotonic interface with atomically thin monolayer tungsten diselenide (WSe2). We fabricate titanium dioxide (TiO2) waveguides directly on the surface of low disorder, boron nitride-encapsulated WS
Distribution Statement: 2-Distribution Limited to U.S. Government agencies only; report contains proprietary info
Acknowledged Federal Support: **Y**

Publication Type: Journal Article Peer Reviewed: Y **Publication Status:** 1-Published
Journal: Nature Photonics
Publication Identifier Type: DOI Publication Identifier: 10.1038/s41566-022-00971-7
Volume: 16 Issue: 4 First Page #: 330
Date Submitted: 8/29/22 12:00AM Date Published: 3/1/22 12:00AM
Publication Location:
Article Title: Electrically controllable chirality in a nanophotonic interface with a two-dimensional semiconductor
Authors: Robert Shreiner, Kai Hao, Amy Butcher, Alexander A. High
Keywords: Nanophotonics, Optical materials, Photonic devices, 2D materials, Nonreciprocal
Abstract: Chiral nanophotonic interfaces enable propagation direction-dependent interactions between guided optical modes and circularly dichroic materials. Electrical tuning of interface chirality would aid active, switchable non-reciprocity in on-chip optoelectronic and photonic circuitry, but remains an outstanding challenge. Here, we report electrically controllable chirality in a nanophotonic interface with atomically thin monolayer tungsten diselenide (WSe2). Titanium dioxide waveguides are directly fabricated on the surface of low-disorder, boron nitride-encapsulated WSe2. Following integration, photoluminescence from excitonic states into the waveguide can be electrically switched between balanced and directionally biased emission. The operational principle leverages the doping-dependent valley polarization of excitonic states in WSe2. Furthermore, the nanophotonic waveguide can function as a near-field source for diffusive exciton fluxes.
Distribution Statement: 1-Approved for public release; distribution is unlimited.
Acknowledged Federal Support: **Y**

Publication Type: Journal Article Peer Reviewed: **Publication Status:** 1-Published
Journal: Nature Nanotechnology
Publication Identifier Type: DOI Publication Identifier: 10.1038/s41565-022-01140-1
Volume: 17 Issue: 6 First Page #:
Date Submitted: Date Published: 5/12/22 12:00AM
Publication Location:
Article Title: Author Correction: Robotic four-dimensional pixel assembly of van der Waals solids
Authors: Andrew J. Mannix, Andrew Ye, Suk Hyun Sung, Ariana Ray, Fauzia Mujid, Chibeom Park, Myungjae Le
Keywords: Electrical and Electronic Engineering
Abstract:
Distribution Statement: 1-Approved for public release; distribution is unlimited.
Acknowledged Federal Support:

Publication Type: Journal Article Peer Reviewed: Y **Publication Status:** 1-Published
Journal: Nature Nanotechnology
Publication Identifier Type: DOI Publication Identifier: 10.1038/s41565-021-01061-5
Volume: 17 Issue: 4 First Page #:
Date Submitted: 9/11/23 12:00AM Date Published: 1/24/22 5:00AM
Publication Location:
Article Title: Robotic four-dimensional pixel assembly of van der Waals solids
Authors: Andrew J. Mannix, Andrew Ye, Suk Hyun Sung, Ariana Ray, Fauzia Mujid, Chibeom Park, Myungjae Le
Keywords: Electrical and Electronic Engineering
Abstract: Van der Waals (vdW) solids can be engineered with atomically precise vertical composition through the assembly of layered two-dimensional materials1,2. However, the artisanal assembly of structures from micromechanically exfoliated flakes3,4 is not compatible with scalable and rapid manufacturing. Further engineering of vdW solids requires precisely designed and controlled composition over all three spatial dimensions and interlayer rotation. Here, we report a robotic four-dimensional pixel assembly method for manufacturing vdW solids with unprecedented speed, deliberate design, large area and angle control. We used the robotic assembly of prepatterned ‘pixels’ made from atomically thin two-dimensional components. Wafer-scale two-dimensional material films were grown, patterned through a clean, contact-free process and assembled using engineered adhesive stamps actuated by a high-vacuum robot. We fabricated vdW solids with up to 80 individual layers, consisting of 100?×?100??m2 areas w
Distribution Statement: 2-Distribution Limited to U.S. Government agencies only; report contains proprietary info
Acknowledged Federal Support: **Y**

CONFERENCE PAPERS:

Publication Type: Conference Paper or Presentation **Publication Status:** 1-Published
Conference Name: APS March Meeting
Date Received: 14-Sep-2023 Conference Date: 14-Mar-2022 Date Published: 14-Mar-2022
Conference Location: Chicago
Paper Title: Electrically controllable chirality in a nanophotonic interface with a 2D semiconductor
Authors: Shreiner, Robert, Hao, Kai, Butcher, Amy, High, Alexander
Acknowledged Federal Support: **Y**

Publication Type: Conference Paper or Presentation **Publication Status:** 1-Published
Conference Name: APS March Meeting
Date Received: 14-Sep-2023 Conference Date: 05-Mar-2023 Date Published: 05-Mar-2023
Conference Location: Las Vegas
Paper Title: Chiral nanophotonic interfaces for near-field optical control of two-dimensional semiconductors
Authors: Robert Shreiner, Kai Hao, Andrew Kindseth, Alexander High
Acknowledged Federal Support: **Y**

Publication Type: Conference Paper or Presentation **Publication Status:** 1-Published
Conference Name: APS March Meeting
Date Received: 14-Sep-2023 Conference Date: 14-Mar-2022 Date Published: 14-Mar-2022
Conference Location: Chicago
Paper Title: Optically controllable magnetism in atomically thin semiconductors
Authors: Kai Hao, Robert Shreiner, Andrew Kindseth, Alexander High
Acknowledged Federal Support: **Y**

RPPR Final Report
as of 18-Sep-2023

Publication Type: Conference Paper or Presentation **Publication Status:** 1-Published
Conference Name: APS March Meeting
Date Received: 14-Sep-2023 Conference Date: 05-Mar-2023 Date Published: 05-Mar-2023
Conference Location: Las Vegas
Paper Title: Optical investigation of magnetic order in monolayer semiconductors
Authors: Kai Hao, Robert Shreiner, Andrew Kindseth, Alexander High
Acknowledged Federal Support: **Y**

Publication Type: Conference Paper or Presentation **Publication Status:** 1-Published
Conference Name: SPIE Photonics West
Date Received: 14-Sep-2023 Conference Date: 02-Feb-2023 Date Published: 17-Mar-2023
Conference Location: San Francisco
Paper Title: Electrically controllable chirality in a nanophotonic interface with a 2D semiconducto
Authors: Robert Shreiner, Kai Hao, Amy Butcher, Andrew Kindseth, Alexander High
Acknowledged Federal Support: **Y**

Partners

,

I certify that the information in the report is complete and accurate:
Signature: Alexander Arthur High
Signature Date: 9/14/23 9:31AM

Final Report, due September 14th, 2023

Proposal Number: 76832-EL, Agreement Number: W911NF-20-1-0217

PI: Alexander High, University of Chicago Pritzker School of Molecular Engineering

Abrstract: This research explored new modalities to break time reversal symmetry in two-dimensional (2D) materials towards the realization of non-reciprocal integrated photonics and optical control of solid state memories. The first objective of the research was to investigate new device architectures to enable optically-driven, on-chip nanophotonic isolators with micron-scale footprints and low power requirements for control. These devices are critical the development of compact LIDAR and other important photonic technologies. By using optical drives and micron-scale photonics structures instead of magnets and millimeter-scale photonic structures, we seek to significantly improve the integration of these devices. Our methodology relies on optical spin-orbit coupling (OSOC) in nanophotonic structures coupled to 2D materials as a mechanism to break time-reversal symmetry and enable isolation. While, there are other actively-investigated approaches to generating non-reciprocity in photonics without magnetic fields, such as topological photonics, balanced gain-loss systems, electro-optic modulators, and coupled non-near oscillators, we explored an approach is intrinsically simple and compact, and utilizes micron-scale ring- and disk-resonators and linear driving fields to create new technologies. Over the course of the research, we made the following critical advances towards realizing non-reciprocal integrated photonics: (1) Establishing a tunable, chiral nanophotonic interface with 2D materials (2) Demonstrated local driving of spin-polarized excitons through the waveguide (3) Established a scalable pathway for integration of titanium dioxide nanophotonic waveguides and resonators with 2D materials with no observable degradation to the 2D materials (4) Fine-tuned our fabrication of resonators and waveguides to maximize interaction with the 2D materials while maintaining high quality factors. The second objective of this research was to determine if integrated photonics can optically-control magnetic solid-state memories. Such control would advance optical computing and interconnects by creating a new photonic interface with traditional solid state electronic computing. Specifically, we sought to determine if OSOC can control spin magnetism in electronically-doped TMDCs. Over the course of the proposal we made the following advances in this direction: (1) We observed that we can optically drive magnetism in electrons in 2D materials with microwatt level optical pumps. This magnetism creates a large circular dichroism in the material – indeed, the excitonic resonances can be up to %90 circularly polarized. (2) Demonstrated that optical pumps in photonic waveguides can generate circular dichroism in 2D materials, another essential step towards realizing isolation. While we were unable to realize our goal of optical isolation, our advances in integrated photonics and advances in optically-controllable magnetism have set the stage for the next phase of research that leverages the low-power control of optical memories and additional material engineering to build optical logic using photonic interfaces with 2D materials. Our results were disseminated in manuscripts in *Nature Photonics* and *Science Advances*, and we also filed a patent on our capabilities to optically-control magnetic order.

Objectives for the entire research project: The first objective of this research is to leverage optical spin-orbit coupling (OSOC) in photonic structures to optically-drive magnetic phenomena in semiconducting transition metal dichalcogenides (TMDs) and in turn generate on-

chip isolation. TMDs host optical exciton transitions with exceptionally large oscillator strengths and valley-dependent circular polarization. We are able to create intense, circularly-polarized optical fields in photonic ring resonators with moderate input powers. In direct proximity to the resonator, TMDs will interact with the chiral fields. One interaction mechanism is the valley-dependent optical Stark effect (OSE). We have performed a full numerical analysis of this interaction that combines simulations of optical fields and experimentally-measured quality factors of photonic cavities with known material properties of TMDs. We calculated that we with ~ 10 milliwatts of driving power, we can optically-drive energetic spin splitting of exciton transitions in TMDs of 16 meV or greater - equivalent to placing the material in a 100 Tesla magnetic field. This interaction would breaks time-reversal symmetry in the TMD, and enable all-optical on-chip isolation in integrated photonics. While we were unable to achieve the input laser power necessary to reach the non-linear optical Stark effect regime, due to less-than-simulated coupling efficiency from the far-field, we uncovered an additional interaction mechanism that can be leveraged for generating isolation and other non-reciprocal effects with significantly lower driving powers. We have observed that we can optically drive magnetism in electrons in 2D materials with microwatt level optical pumps (this is also discussed in the secondary objective below). This magnetism creates a large circular dichroism in the material – indeed, the excitonic resonances can be up to %90 circularly polarized. This large dichroism can be applied to isolation, and we are eagerly exploring this avenue in the next phase of research.

The second goal of this research proposal is to determine if OSOC in integrated photonics can optically control magnetic solid-state memories. Specifically, we will determine if OSOC can control spin magnetism in electronically-doped TMDs. This research can break new ground in our ability to control spins in solid-state materials. If successful, the same techniques can be applied directly to more commonly utilized magnetic thin films. Such control would advance optical computing and interconnects by creating a new photonic interface with traditional solid state electronic computing. Beyond improved integration possibilities, optically driven magnetism offers additional advantages over traditional magnetic systems, including to the capability to be reconfigured at ultra-fast timescales, enabling dynamic control, and memory control without energy consuming electronics. Additionally, the magnetic state can also exhibit strong circular dichroism. This can be additionally leveraged for isolation.

Timeline*:* Our accomplishments will be discussed in depth in the following section, but here we briefly describe the proposed research timeline and completion percentage. We note that while we were not able to fully complete objective 1, we were able to accomplish all major goals of objective 2.

Towards objective 1, we set the following targets: Target 1 (75% completed) for years 1 and 2: Generation and Mapping of the optical Stark Effect. Target 2 (50% completed) for years 2-3: Generation of optical isolation. Target 3 (50% completed) for year 3: Optimization of isolation and exploration of broader wavelength regimes

Towards objective 2, we set the following targets: Target 1 (100% completed) for Years 2 and 3: Optical control and mapping of spin populations. Target 2 (100% completed) for year 3: Dynamic control of spin and magnetism.

Summary of findings for objective 1: On Chip, Optically Driven Isolators

Key findings described in the text below: (1) Established a scalable pathway for integration of titanium dioxide nanophotonic waveguides and resonators with 2D materials with no observable degradation to the 2D materials (2) Established a tunable, chiral nanophotonic interface with 2D materials, detailed in our publication in Nature Photonics (3) Demonstrated local driving of spin-polarized excitons through the waveguide (4) Fine-tuned our fabrication of resonators and waveguides to maximize interaction with the 2D materials while maintaining high quality factors.

Background: Photonic structures exhibiting OSOC can be coupled with chiral optical materials – i.e., materials that interact selectively with circularly polarized light – to generate chiral light-matter interfaces. Such interfaces create light-matter interactions that depend on the propagation direction of light and provide a foundation for new photonic and plasmonic technologies, such as on-chip beam splitting for circularly polarized input light and optically driven optical isolation[1].

An emerging platform for these chiral optical interfaces are TMDCs. TMDC monolayers are direct bandgap semiconductors with optical resonances in the visible and near-infrared range dominated by excitonic states. Due to broken inversion symmetry in the monolayer crystal lattice, two inequivalent sets of bandgap minima exist at the momentum space K points (i.e., K and K' valleys), which couple to light of opposite helicity. Preliminary demonstrations with plasmonic, nanowire, and photonic crystal systems have shown the feasibility of coupling light to TMDC valley excitonic states through OSOC. However, the scalable, deterministic incorporation of such architectures in existing integrated photonic platforms is challenging to achieve. Moreover, the chiral TMDC interfaces demonstrated so far are passive. A scalable nanophotonic-TMDC interface equipped with active electrical tunability could enable new applications in optoelectronic and integrated photonic technologies. Valley polarization, which characterizes the chiral response of TMDCs, can be modified by electrostatic doping, providing an avenue for active control. Additionally, in monolayer TMDCs the exciton valley index determines the spin configurations of the underlying charge carriers in charged excitonic state. Therefore, a photonic-TMDC interface also opens the opportunity to control semiconductor spins with integrated photonics, enabling nanoscale optical manipulation of solid-state memories.

(1) Photonics integration with 2D materials: Over the course of the funding, we have built an interface which exploits these unique material properties to realize electrically tunable chirality. The interface is based on deterministic fabrication of nanophotonic structures on arbitrary substrates and can be applied to a range of devices, facilitating broader application of chiral interfaces in nanophotonic circuitry. Our device consists of a titanium dioxide (TiO2) nanophotonic waveguide fabricated on a hexagonal boron nitride (hBN)-encapsulated tungsten diselenide (WSe2) monolayer (Fig. 1a). Encapsulation with hBN significantly reduces inhomogeneity in TMDCs and serves as a dielectric for electrostatic tuning. Electrical control is achieved with few-layer graphene back-gate and contact flakes. We fabricate TiO2 waveguides on top of these heterostructures using templated atomic layer deposition. This fabrication method produces low-loss nanophotonic structures (Fig. 1b) without damaging the underlying substrate, making it ideal for interfacing with two-dimensional materials. Following waveguide fabrication,

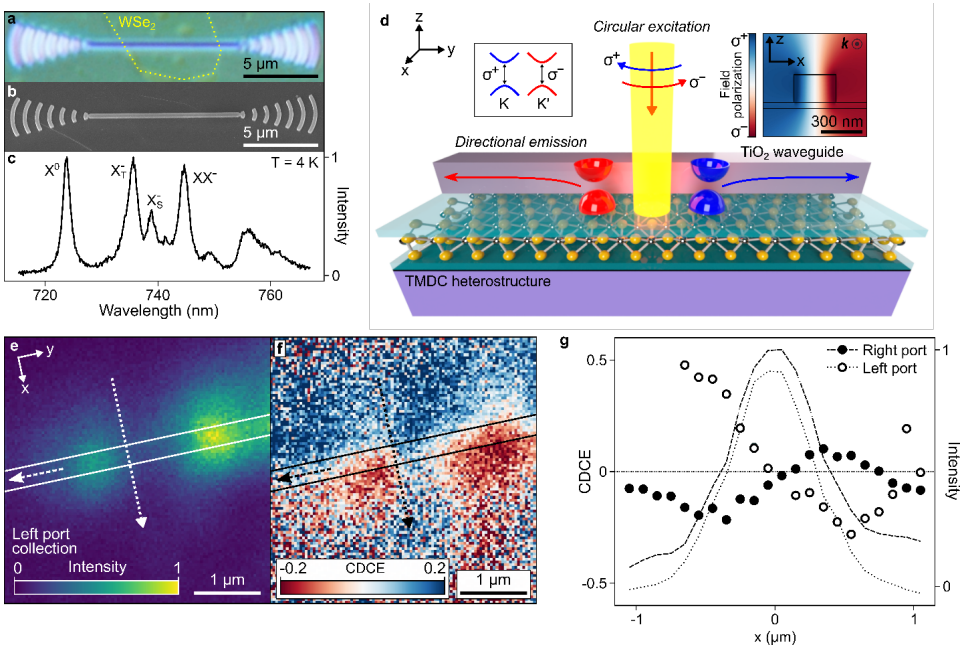

Figure 1 | Chiral nanophotonic-TMDC interface. a,b, (a) Optical and (b) scanning electron microscope images of the TMDC-waveguide interface. c, PL of encapsulated WSe2 at 4K shows prominent exciton, trion and charged biexciton peaks. d, Schematic depicting chiral-directional coupling. Left inset: Chiral optical selection rules of monolayer TMDCs. Right inset: Chiral electric field intensity distribution of waveguide mode propagating out of the page. e, Spatial mapping of PL intensity measured through the left port under linear far-field excitation. f, Spatial mapping of CDCE through the left port under circular far-field excitations. g, Line cuts of CDCE across the waveguide along the dashed arrow direction in e and f for left (open circles) and right (solid circles) ports.

the WSe2 monolayer exhibits narrow linewidth excitonic emission (Fig. 1c), confirming that our photonic integration process generates minimal inhomogeneities in the van der Waals heterostructure and is suitable for photonic integration with TMDCs.

Our newly developed fabrication method enables deterministic, scalable integration of photonics with two-dimensional materials, where device geometry and circuitry size are limited only by the constraints of advanced lithography and the component material systems. Our method can be utilized to integrate photonics with wafer scale CVD TMDCs and hBN. Our interface opens new opportunities for exploring the intersection of nanophotonics and two-dimensional materials, as shown here in our novel reports of gate-controlled photonic chirality and near-field driving of valley(spin)-polarized exciton fluxes. Combined with recent advances in large area growth and exfoliation of two-dimensional materials, this work establishes a universal platform for their scalable integration with on-chip nanophotonic circuitry. Following our device engineering, we do not foresee barriers for ourselves or other research groups to implementing our technologies at the wafer-scale.

(2) Experimental investigation of chiral light-matter interface: Figure 1d illustrates the directional coupling that emerges between the waveguide modes and the TMDC material from their respective chiral characteristics. The electric field distribution of the propagating TE mode is tightly confined (waveguide width < λ/2), manifesting in-plane, circularly polarized evanescent fields (Fig. 1d, right inset). The sign of the polarization (right-handed σ+ or left-

handed σ-) inverts across the waveguide and with propagation direction. Depending on location, excitons in the K and K' valleys (Fig. 1d, left inset) will selectively couple to left- or rightward propagating modes of the waveguide, thus establishing chiral-directional coupling at the waveguide-monolayer interface.

To characterize the interface, we first generate excitons and observe their radiative emission into the guided optical modes of the waveguide. The monolayer is excited from the far-field by a 660 nm laser. Excitonic photoluminescence (PL) couples to the waveguide and is detected by collecting the light scattered from gratings at the waveguide ends. Figure 1e displays the measured PL intensity from the left port when a linearly polarized excitation is scanned around the waveguide. To study the chiral-directional coupling, we switch the polarization of the excitation laser from linear to circular, σ+ and σ-, creating valley-polarized excitonic states that preferably emit with the same polarization as the excitation (Fig. 1d). We characterize the interface by the chiral-directional coupling efficiency CDCE (x,y) = [I (x,y) σ+ - I (x,y) σ-] / [I (x,y) σ+ + I (x,y) σ-], where I(x,y)σ+(σ-) is the PL intensity measured from a specific port under σ+(σ-) excitation at position (x,y). Figure 1f shows the spatial mapping of the CDCE for left port collection. As anticipated, we observe that the sign of the CDCE inverts as the excitation spot crosses the waveguide, approaching a magnitude of 20%, and that the sign of the CDCE flips between the two outcoupling ports (Fig. 1g). We also note that under linearly polarized excitation, the chiral-directional coupling vanishes as expected. For both ports, the CDCE goes to zero near the center of the waveguide, where the mode polarization is linear (Fig. 1d, right inset). Far from the waveguide center, the CDCE also falls to zero as low-signal noise dominates. These experimental signatures directly verify the predicted chiral interface between the TMDC monolayer and photonic waveguide.

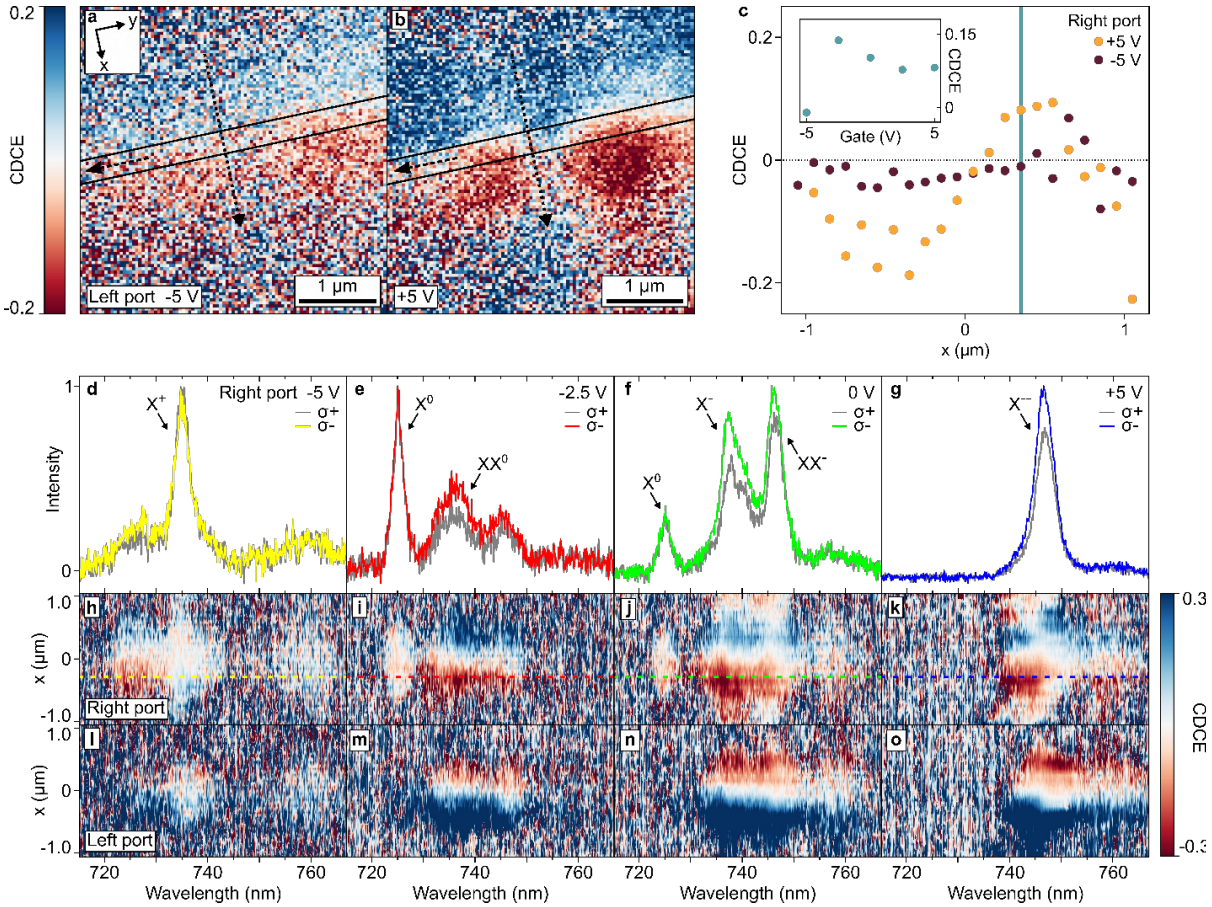

Figure 2 | Electrostatic tuning of interface. a,b, Spatial mapping of CDCE of emission collected through left port under applied gate biases of (a) -5 V and (b) 5 V. c, Line cuts of CDCE of emission collected through right port along the dashed arrow direction in a and b. Inset: Gate dependence of CDCE at x = +300nm (blue vertical line in c). d-g, PL out-coupled from right port under selected gate voltages with σ+ and σ- excitations fixed at x ≈ -300 nm. Excitonic states are labeled. h-k (l-o), Spectrally resolved spatial mapping of right (left) port CDCE at selected voltages. Dashed lines indicate the corresponding spectra line cuts in d through g.

The integration of contacts and electrodes in our device architecture allows us to electrically dope the TMDC monolayer and, in turn, potentially control the chirality of our integrated photonic interface. To study this tunability, we apply a gate voltage to the TMDC monolayer and investigate the impact to the chiral-directional coupling. Figures 2a-b show the spatially mapped CDCE measured for gate voltages of -5 V and 5 V, respectively. The CDCE significantly diminishes under negative applied bias. Comparing transverse line cuts across the waveguide (Fig. 2c), the CDCE spatial dependence at -5 V flattens to zero, while at +5 V it displays the expected crossing at x = 0. At a fixed displacement of ~300 nm away from the waveguide, we observe a sharp transition in CDCE from near 0% at -5 V to around 15% at -2.5 V (Fig. 2c, inset). This result directly demonstrates active electrical control over the chirality of the TMDC-waveguide interface.

To investigate the electrical tuning in more detail, we perform spectrally resolved measurements of the out-coupled photoluminescence. Figures 2d-g show gate-dependent PL spectra collected from the right grating port for fixed-position off-waveguide σ+ and σ- excitations. We attribute characteristic peaks to neutral and charged exciton and biexciton states delineated in recent literature. Combining this spectroscopic information with the electrostatic control afforded by our high-quality interface, we analyze the chiral-directional coupling for each excitonic state. From the spectra in Figs. 2d-g, we find that the positive trion (X+) and neutral exciton (X0) states display balanced emission into the waveguide independent of the excitation polarization. In contrast, the negative trion (X- and X--) and biexciton (XX0 and XX-) states exhibit directional emission. More completely, Figs. 2h-k(l-o) show the wavelength-resolved right (left) port CDCE versus the position of the excitation beam. Minimal variation is observed for the X+ and X0 peaks, whereas for the X-, X--, XX0 and XX- peaks, the CDCE inverts across the waveguide and reaches magnitudes near 20% on either side. These measurements indicate that the different excitonic states in the monolayer exhibit varying degrees of chiral-directional coupling and that the electrostatic control of this coupling correlates with switching between dominant excitonic states.

To better understand the doping-dependent chiral-directional coupling for different excitonic states, we perform gated far-field photoluminescence measurements of the encapsulated WSe2. Notably, X+ shows no valley polarization, which explains the quenched waveguide coupling in the hole region, while X-T (triplet trion) and X-- show the strongest far-field polarizations, as well as the clearest CDCE signatures. Considering these far-field valley polarization results, we fit the measured CDCE profiles for the excitonic states to simulation and find an isolated interface fidelity as high as 90%.

Our observation of widely differing valley polarizations for different species can be understood by considering the energetics of intervalley scattering for electrons and holes that comprise the charged excitons. For X- (X+), the hole (electron) spin determines the emission polarization and must flip to change the emission helicity. The energy barrier for inter-valley scattering is much larger for holes than for electrons, resulting in different scattering rates and therefore different polarizations of emission for positive and negative trions. The measured results described by these depolarization pictures confirm that the tuning of the chirality in the photonic interface is due to gate modification of the valley dynamics in monolayer TMDCs.

(3) Local generation and control of spin-polarized excitons: In addition to enabling electrical control over chiral-directional coupling of the excitonic emission, the TMDC-waveguide interface opens new possibilities to locally create and manipulate chiral excitons and spins. With

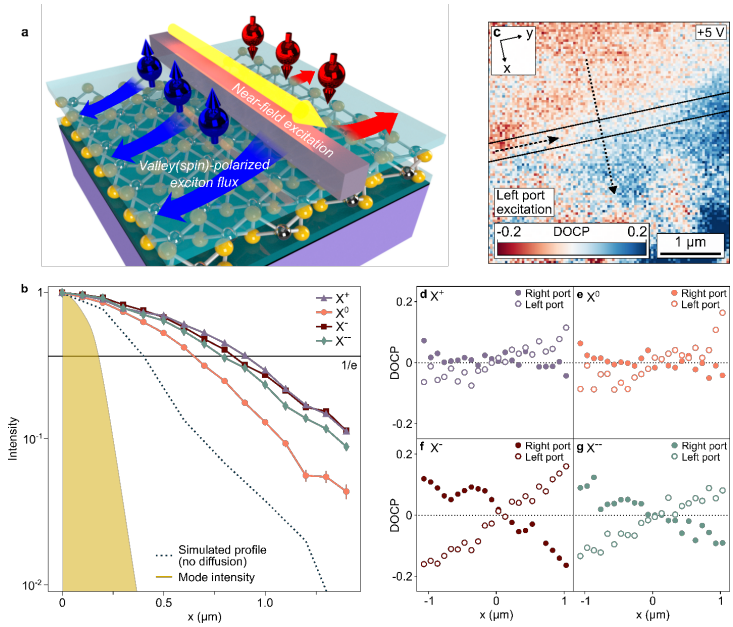

Figure 3 | Photonic pumping of valley(spin)-polarized exciton fluxes. a, Schematic of valley(spin)-polarized exciton flux generation. Outward arrows (blue/red) indicate diffusion of oppositely valley-polarized excitons carrying spins for fixed propagation direction of the waveguide excitation mode (yellow). b, Normalized PL intensity distributions versus distance from waveguide (center at x = 0 μm) for different excitonic states. Shaded area is the simulated electric field intensity profile of the guided mode in the waveguide. Dashed line shows the simulated collection profile in the absence of diffusion given experimental resolution. c, DOCP map under 5 V gate bias, left port excitation, and far-field collection. d-g, DOCP of different excitonic states along the dashed arrow direction in c. Open (solid) circles correspond to rightward (leftward) propagating

improvements in sample quality and the observation of long-lived excitons in heterostructures, exciton diffusion in 2D semiconductors has recently garnered increasing interest, providing a context for fundamental explorations of planar spatial dynamics in systems with many-particle interactions and enabling such optoelectronic technologies as room-temperature excitonic transistors. Unlike in bare, few-layer samples, the encapsulated TMDC monolayers in our interface provide reduced-disorder environments for studying exciton propagation and preserve spin-valley locking, allowing the simultaneous transport of spin-polarized charge carriers. Compared with the far-field optical excitations currently utilized to drive exciton diffusion, the waveguide modes of high-index nanophotonic structures can act as compact, tailored, on-chip sources of exciton fluxes. Moreover, the high degree of circular polarization of their evanescent fields enables the generation of valley-polarized exciton fluxes, which can be directionally reconfigured (Fig. 3a). Therefore, a new modality for injecting spin currents in semiconductors with integrated photonics – as opposed to with conventional ferroelectric contacts – can be realized, promising advancements in optical computing and spintronics.

With our device, we first show that the waveguide can locally generate diffusive excitons. To probe this functionality, we couple the excitation laser into the right grating port and collect photoluminescence emitted from the TMDC monolayer into the far-field. Figure 3b shows the spatial distribution of exciton PL spectrally selected over wavelength regions of interest. The shaded area illustrates the simulated electric field intensity of the waveguide mode. The quickly

decaying evanescent tail implies a large density gradient of the excitonic states generated by the mode, which induces their diffusive transport away from the waveguide. Considering the measured resolution of our collection channel, we compute the anticipated PL spatial distribution in the absence of exciton diffusion (dashed line in Fig. 3b). We find that the profiles of the excitonic states extend beyond this boundary, indicating their diffusion away from the waveguide. For the charged excitons, both negative and positive, we extract 1/e diffusion lengths $L_{X\pm} \approx 0.45$ μm based on the predicted no-diffusion profile. The neutral exciton displays a diffusion length $L_{X0} \approx 0.25$ μm. These diffusion lengths of hundreds of nanometers are comparable to literature values. The excellent sample quality and comprehensive electrostatic control over our interface enable this extraction of state-specific diffusion.

We next examine the valley(spin)-polarization of these near-field driven exciton fluxes. As before, the evanescent fields on either side of the waveguide exhibit opposite circular polarizations and therefore populate excitonic states in opposite valleys (Fig. 3a). To measure this resulting valley polarization, we analyze the circular polarization of the far-field PL. The valley polarization of the excitonic states is characterized by the PL degree of circular polarization $DOCP(x,y) = [I(x,y)\,\sigma+ - I(x,y)\,\sigma-] / [I(x,y)\,\sigma+ + I(x,y)\,\sigma-]$, where $I(x,y)\,\sigma+$ ($\sigma-$) is the $\sigma+$($\sigma-$) component of the PL intensity collected at position (x,y). Figure 3c shows the DOCP measured under left port excitation and 5 V gate bias, confirming the generation of valley-polarized excitonic states. Figures 3d-g display the position-dependent, spectrally resolved DOCP for the respective X+, X0, X-, and X-- peaks. Like the CDCE (Figs. 2d-g) and far-field Pv results, negative trions exhibit a large DOCP, whereas positive trions and neutral excitons show nearly zero DOCP. We also note the presence of prominent dark trion peaks at ~750 nm. Due to their linear out-of-plane dipole moment, dark trions predominantly couple to the TM mode, showing biased DOCP with a spatial profile independent of the excitation port. For negative trions, due to valley-spin locking, the paired hole spin is fixed by the valley index (see Section VI of SI). Thus, spin-polarized holes are injected with the valley-polarized X- and X-- states. With the diffusion measurements described above, we conclude that our chiral photonic interface serves as a directionally reconfigurable source for injecting hole spin currents in atomically thin semiconductors.

(4) Optimizing ring resonator parameters and further refinement of photonics fabrication

Subsection: Redesigning the optical devices to work far from the exciton resonances

Our initial proposal detailed how a ring resonator on resonance with the exciton resonances of WSe_2 could be used to create isolation from differences in absorption. While this approach was effective at achieving the desired isolation, the larger absorption of the device was disadvantageous. From our simulations, near the exciton resonance we expected 20dB isolation with 15dB insertion loss. Over the last year of the project, we have developed a modification to our approach which maintains the expected isolation while reducing absorption. We now use magnetism-induced circularly dichroic differences in the effective index to create isolation through a shift in resonance frequency of the ring resonator. A recent study of monolayer TMDC based tunable photonics demonstrated that electronic gating of TMDCs could induce changes in the refractive index at 1500 nm, hundreds of nanometers from the exciton resonances. This

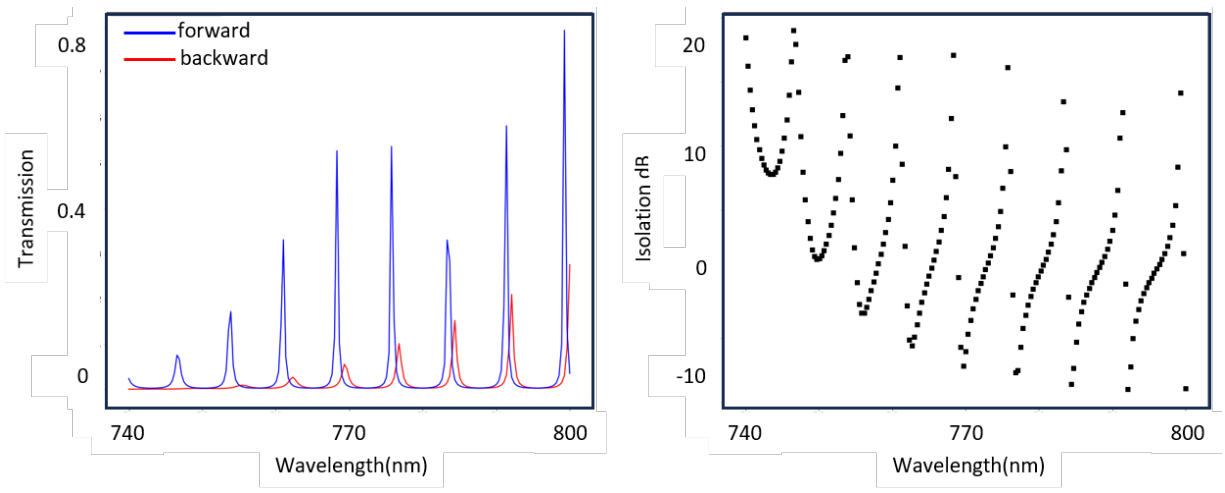

Figure 4: Simulations of isolation for ring resonators red-detuned from the exciton resonance

finding opens new pathways to broadband, tunable 2D material-based photonics. Also, since such tuning avoids the optical resonance of the 2D semiconductor, absorption loss can be significantly reduced. As discussed in the following section on optical control of spins in 2D materials, we can optically generate significant circular dichroism that can manifest as refractive index changes even far from the exciton resonances. From this, we can realize tunable photonic structures.

As a first step towards implementing the new tuning mechanism to our device design, we simulated the structure using the optical response of room temperature WSe2. In addition to improving the efficiency of the device by reducing the absorption loss from the material, the new design also provides broader tuning bandwidth. With the new design, we predict up to 20dB isolation with 5dB insertion loss, see Figure 4. We will pursue this design in the next phase of research.

Subsection: Modifying the photonics integration to optimize operation with the new modality

We further modified our fabrication method allowing us to etch through the layered material structure, followed by nanophotonics integration. In future iterations, by choosing the thickness of the encapsulation hBN layer as well as etching into the substrate below, the waveguide will be accurately buried halfway into the 2D stack. We developed the etching process for integrating TiO2 photonics with layered Van der Waals material without compromising the performance of the nanophotonics. Using electron-beam lithography, geometric patterns are transferred into polymethyl methacrylate (PMMA) resist covering the previously assembled WSe_2 heterostructure. Inductively coupled plasma reactive ion etching is performed with a 1:1 mixture

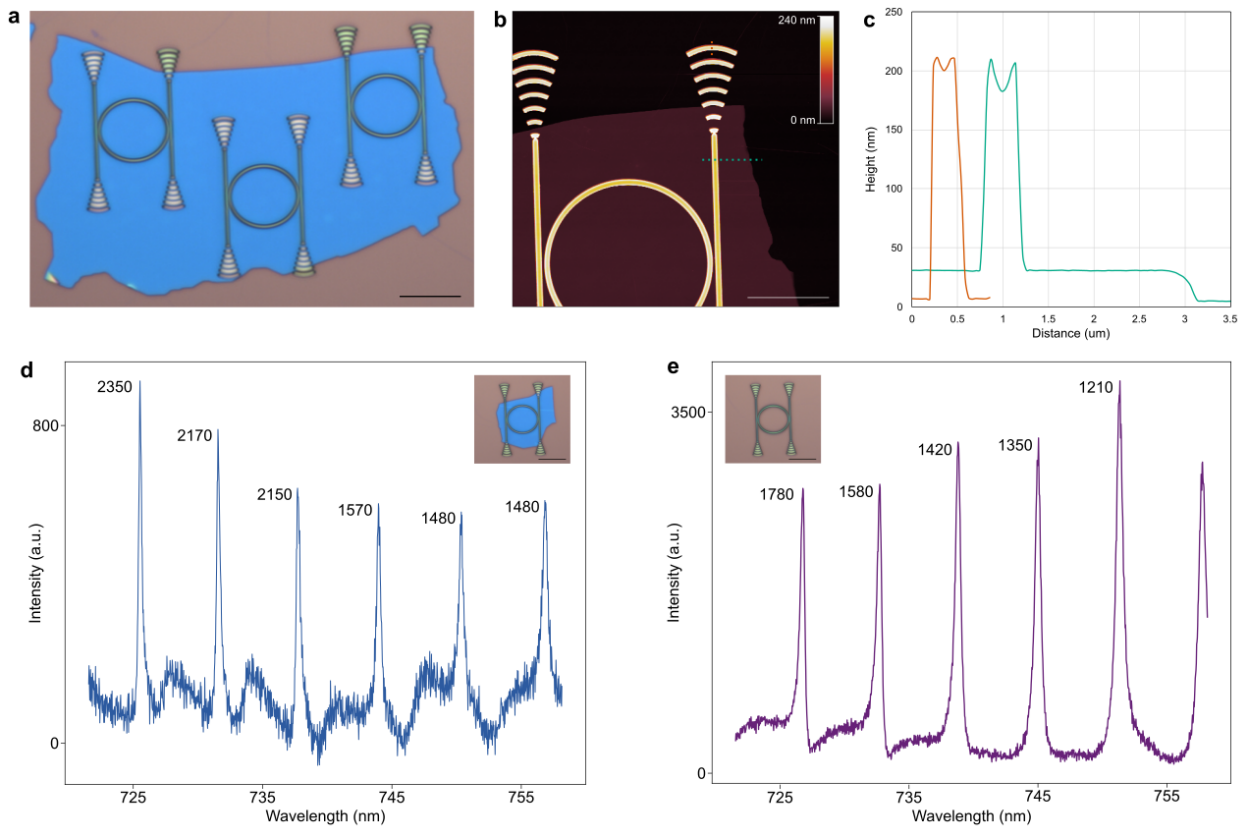

Figure 5: Photonics integration into etched hBN that maintains suitable quality factors.

of SF_6 and Ar. Following the etching step, the trenches are conformally filled with titanium dioxide (TiO_2) via atomic layer deposition. The overgrown TiO_2 is etched away, and the PMMA is rinsed in NMP. The final photonic structure is embedded in the WSe_2

To characterize the performance of the nanophotonic structure, we fabricated ring resonators. Figure 5a shows the optical image of the ring resonators embedded in BN flake. The BN flake is fully etched through with the etching process described in the previous section. Figure 5b depicts the AFM image of an exemplary ring resonator structure. We measured the height of the structure on (green linecut) and off (red linecut) the BN flake. The height of the them are identical as depicted in Figure 5c. It confirms the fully etch of the BN underneath the waveguide. We further characterize the optical performance of the ring resonators by measuring the Q- factor of the resonances. In Figure 5c and d, we compare the Q factor of the rings embedded in BN(c) and on bare chip (d). The ring resonators embedded in BN exhibit ~2000 Q-factor which is slightly better than the quality factor on a bare chip. This demonstration confirms our new fabrication process preserves the high quality of the photonic structure while allowing us to optimize the coupling to excitons and spins in the 2D material.

Summary of findings for Objective 2 – "On-chip optical control of spin populations in TMDs":

Key findings: (1) We observed that we can optically drive magnetism in electrons in 2D materials with microwatt level optical pumps. This magnetism creates a large circular dichroism in the material – indeed, the excitonic resonances can be up to %90 circularly polarized. This is detailed in our publication in Science Advances. We also explored the temporal dynamics of the magnetic ordering (2) We demonstrated that optical pumps in photonic waveguides can generate circular dichroism in 2D materials, another essential step towards realizing isolation. Overall, we met our goals in this objective.

Our findings are detailed in this section. Overall, our findings will accelerate technological developments utilizing TMDCs, already a leading material platform for investigating next-generation spin-, valley-, and optoelectronics. Specifically, the discovery of optically-reconfigurable magnetism and circular dichroism in atomically thin semiconductors will stimulate the design of non-reciprocal optoelectronics and photonics, such as on-chip all-optical isolators with built-in optical memory. Lastly, our research creates a bridge between magnetism and optical control in TMDCs, which can be leveraged for direct interfacing between integrated photonics and magnetic solid-state memories, suggesting new routes for neuromorphic optical computing. These findings were reported in *Science Advances*, and we also filed a patent application on optical control of magnetic memories.

Background: Due to favorable material properties and tuning capabilities, TMDCs are a rapidly emerging platform for the study and manipulation of collective phases in 2D materials. These collective phases, such as magnetic phases, can be leveraged in the development of new technologies. Recently, experiments have shown that under applied magnetic field and in certain doping regimes, electrons in molybdenum disulphide (MoS2) and molybdenum diselenide (MoSe2) exhibit magnetic order with near-complete spin-polarization far beyond the predictions of a simple thermal population model. The spin polarization manifests as circular dichroism in reflectivity and photoluminescence measurements of the excitonic states, and was initially attributed to an interaction-enhanced electronic g-factor (so-called giant paramagnetism) or the emergence of ferromagnetic order. In the ferromagnetism model, the spin polarization is due to strong exchange interactions which favor the formation of a spin-polarized state in both the K and K’ valleys. Follow-up experiments demonstrated that the system transitions from a ferromagnetic to a paramagnetic phase with increased doping, suggesting direct electronic control over the electron-electron interactions and correlated phases. These studies present compelling evidence that the magnetic ordering at moderate carrier densities is ferromagnetic in nature and that spin-polarized electronic states should persist even at zero magnetic field. However, while ferromagnetic order could be expected at zero applied magnetic field, no net magnetization or spin polarization was observed. This absence was attributed to the lack of a global symmetry breaking mechanism.

Optical pumping is a conceivable mechanism to break the symmetry between equivalent spin configurations in TMDs. Recent studies have shown that pumping individual monolayers or heterostructures of TMDs with circularly polarized light can generate spin imbalances with microsecond-long relaxation times. For WSe2 monolayers in the electron doped region, which is the main focus of this work, resident electrons can be dynamically spin/valley-polarized by

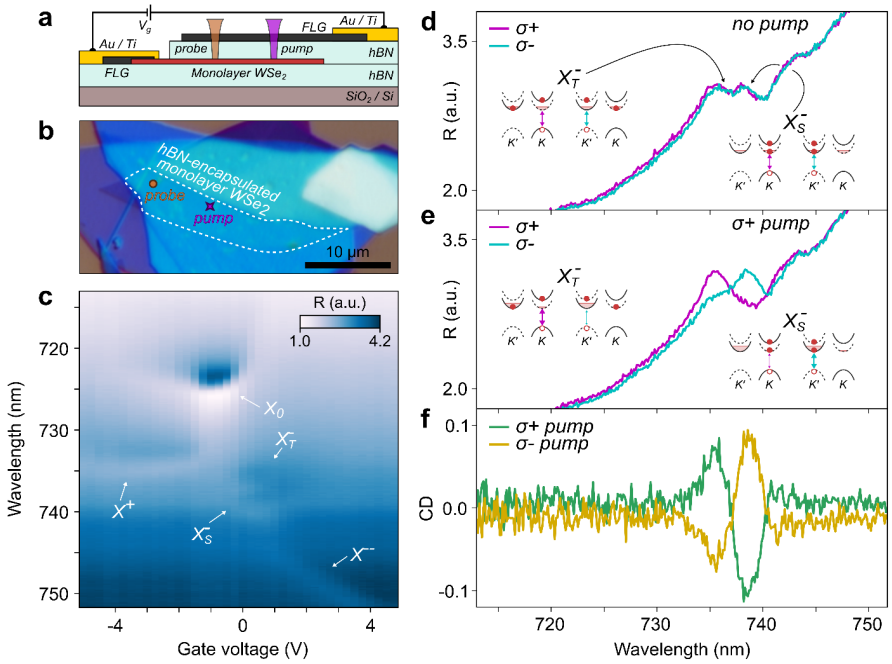

Figure 6: Sample under study. a, Schematic of hBN-encapsulated WSe2 monolayer with few-layer graphene top gate and contacts. The optical pump and probe are spatially separated. b, Optical microscope image of sample D1. c, Gate dependent reflection spectra of the WSe2 sample. The excitonic resonance features are labeled correspondingly. d, σ+ and σ- reflection spectra at 0.5 V, where the singlet and triplet trion features are well resolved. Inset: Singlet and triplet trion configurations showing balanced valley populations. e, σ+ and σ- reflection spectra at 0.5 V under σ+ pumping. Insert: Schematic of singlet and triplet trion in optically pumped spin/valley-polarized electron bath. f, Circular dichroism (CD) spectra under σ+ and σ- pumping. T = 4 K and

continuous pumping with circular light. Photo-generated electrons excited in a selected valley by the circularly polarized pump will preferentially relax to the opposite valley due to fast spin-conserving intervalley scattering. Additionally, the intravalley recombination of resident electrons with photo-generated holes forming dark excitons can enhance the asymmetry of the valley populations. The resulting spin-polarization is maintained in the presence of the continuous pump as these processes occur on timescales faster than the spin relaxation rate. Moreover, due to the relatively low free charge carrier densities n ≈ 10^{12} - 10^{13} cm^{-2}, a significant population of resident carriers may be spin-polarized, potentially sufficient to break the symmetry between ground-state spin configurations and stabilize the ferromagnetic order.

(1) Optical control of magnetic phases: We studied the impact of above-bandgap, circularly polarized optical pumping on h-BN encapsulated monolayers of WSe2. The heterostructure layout and optical image of the sample D1 are presented in Figures 6a and 6b. The doping level in the monolayer can be controlled by applying gate voltage between the few-layer graphene contact and top gate and manifests in the appearance of neutral and charged excitonic resonances in the reflection spectra, Figure 6c. We first focus on low temperature measurements at T = 4 K within the moderately electron-doped region, where singlet (X-S) and triplet (X-T) trions are clearly observed. Reflection from a circularly polarized supercontinuum laser provides a probe of the local, valley-selective optical response. In the absence of pumping, balanced reflection of σ+ and σ- polarized light is observed (Fig. 6d), indicating that the probe laser does not generate

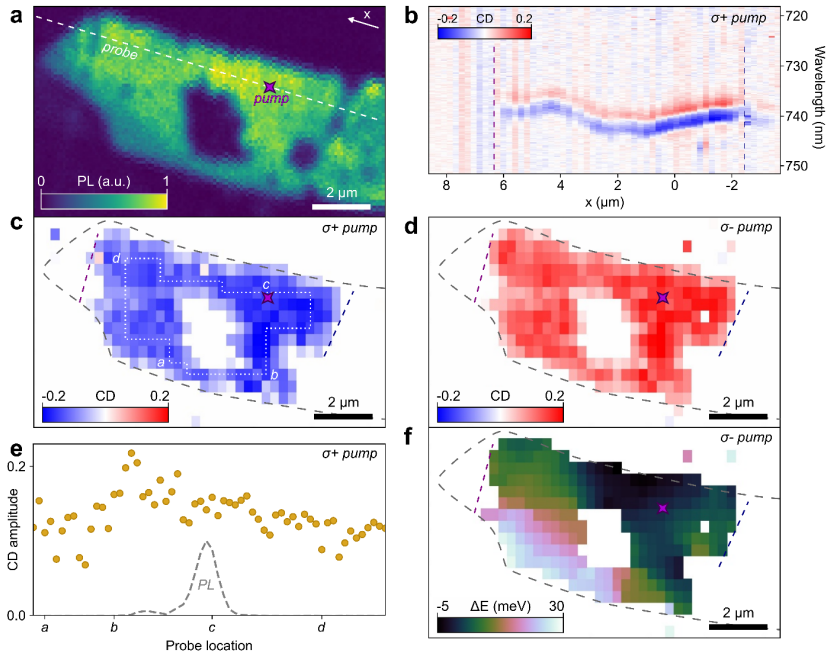

Figure 7: Spatial profile of the spin polarization. a, Photoluminescence (PL) map of the ROI. b, Spatially dependent CD spectra under σ+ pumping. The fixed pump location x = 0 µm is given by the star in (a), while the probe is scanned along the dashed white line in (a). c,d, Map of the CD amplitude across the whole ROI under σ+(c) and σ-(d) pumping. e, CD amplitude along the dashed contour in (c). Dashed gray line depicts the PL intensity for fixed-position pumping. f, Map of peak energy shifts of the singlet CD signal compared to the value at the pump location. Purple and blue dashed lines correspond to wrinkles on the sample. T = 4 K and pump

any symmetry breaking. Next, we pump the sample with a 660 nm diffraction-limited continuous wave laser with a spot diameter of 500 nm and a power of 7.8 µW. To demonstrate the nonlocality of pump-induced effects and to eliminate the influence of photoluminescence in detection, the probe spot is separated by nearly 8 µm from the pump (Fig. 6b). The reflection spectra under σ+ polarized pumping are markedly different – the triplet (singlet) trion dominates the probe signal co(cross)-polarized to the pump (Fig. 6e). This pump-induced circular dichroism is characterized by CD = ΔR+ - ΔR-, where ΔR+,- = (R+,-on / R+,-off) – 1 is the differential reflectivity comparing the σ+,- probed reflection in the presence (R+,-on) and absence (R+,-off) of the pump. The CD signal displays amplitudes approaching 10% and inverts with the sign of the pump polarization (Fig. 6f).

The CD is a direct signature of electron spin/valley-polarization, in which singlet and triplet trions are formed preferably in the opposite valleys (see Fig. 6e inset). To quantify the spin polarization, we determine the valley-dependent oscillator strengths of the trion states by fitting the reflection contrast with a Breit-Wigner-Fano lineshape. Since the valley-dependent charge density correlates with the oscillator strength of the transition, we estimate that 90%(10%) of charges reside in the valley cross(co)-polarized with the pump even at 8 µm pump-probe separation. This corresponds to a spin polarization Ps = 0.77, where Ps = (A+ - A-) / (A+ + A-) and A+,- is the probe-polarization-selective oscillator strength of the trion state under optical

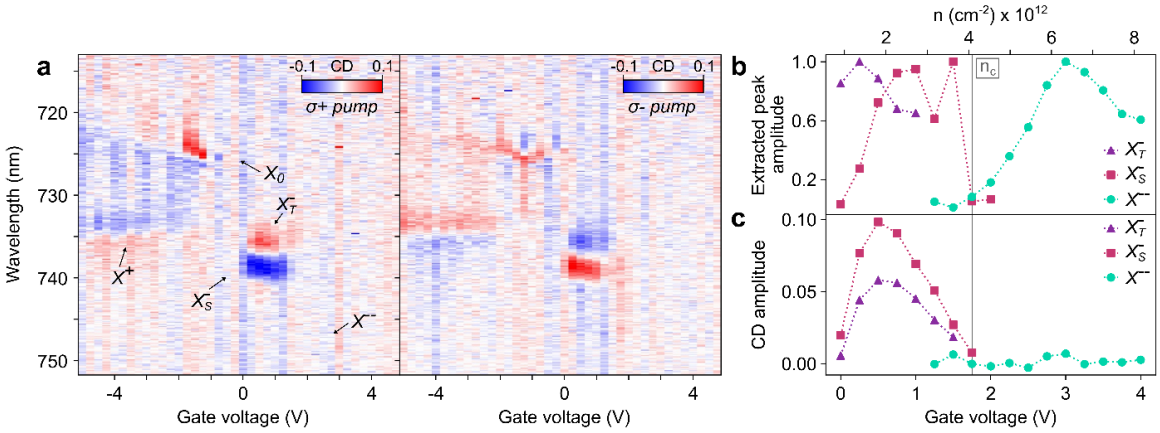

Figure 8: Gate dependence of CD spectra. a, Gate dependent CD spectra probed 8 μm from the pump (Fig. 1b) under σ+ (left) and σ- (right) pumping. Excitonic states are labeled corresponding to the features in reflection spectra. b, Extracted peak amplitude versus gate voltage (doping level). c, CD amplitude versus gate voltage (doping level). The critical electron density nc is indicated. T = 4 K and pump power is 7.8 μW.

pumping. For an electron doping density of $n \approx 1.8 \times 10^{12}$ cm^{-2} (see Supplementary Information), this yields a spin population imbalance of $\sim 1.4 \times 10^4$ μm^{-2}. Small disparities in the local optical environment and sample inhomogeneity may subtly modify the relationship between the CD signal and the underlying spin polarization, however, this extracted value provides a reasonable approximation.

Remarkably, the optical pump generates a near-complete spin polarization that persists micrometers away from the pump location. We next study this spatial dependence in more detail. Figure 7a shows a photoluminescence (PL) map of the region of interest (ROI) of the monolayer flake. The central dark area corresponds to a bilayer region. Keeping the pump at the fixed point x = 0 μm (star in Fig. 5a), the probe is scanned along the length of the monolayer (dashed line in Fig. 5a). Strong CD signal is detected, reaching an amplitude of 20% (Fig. 5b). Moreover, the CD signal shows significant energetic variation, indicating that the spin polarization is robust to sample inhomogeneity. These observations imply the maintenance of long-range spin polarization built up under circularly polarized optical pumping.

To further characterize the spatial profile of the spin polarization, we map the CD signal across the entirety of the ROI. Figure 7c depicts the CD associated with the singlet trion peak as the probe is scanned across the flake while the σ+ pump remains fixed. CD is clearly observed within the pristine portion of the ROI, except for in the bilayer region where no resonance peak nor CD signal are found. When the sign of the pump polarization is flipped to σ- (Fig. 7d), the CD signal inverts everywhere. To investigate the correlation between the pump-probe displacement and the CD intensity, we plot a cross section of the CD amplitude around the ROI (Fig. 7e). No clear CD signal decay is observed as the separation increases. Indeed, in the c to b direction, we observe an increase in CD signal. The spatial inhomogeneity of the sample is depicted in Figure 7f. The trion resonance energy varies by up to 30 meV within the ROI, while the CD signal is still robust. However, more prominent imperfections apparently destroy the spin polarization. The purple and blue dashed lines indicate wrinkles and residue in the

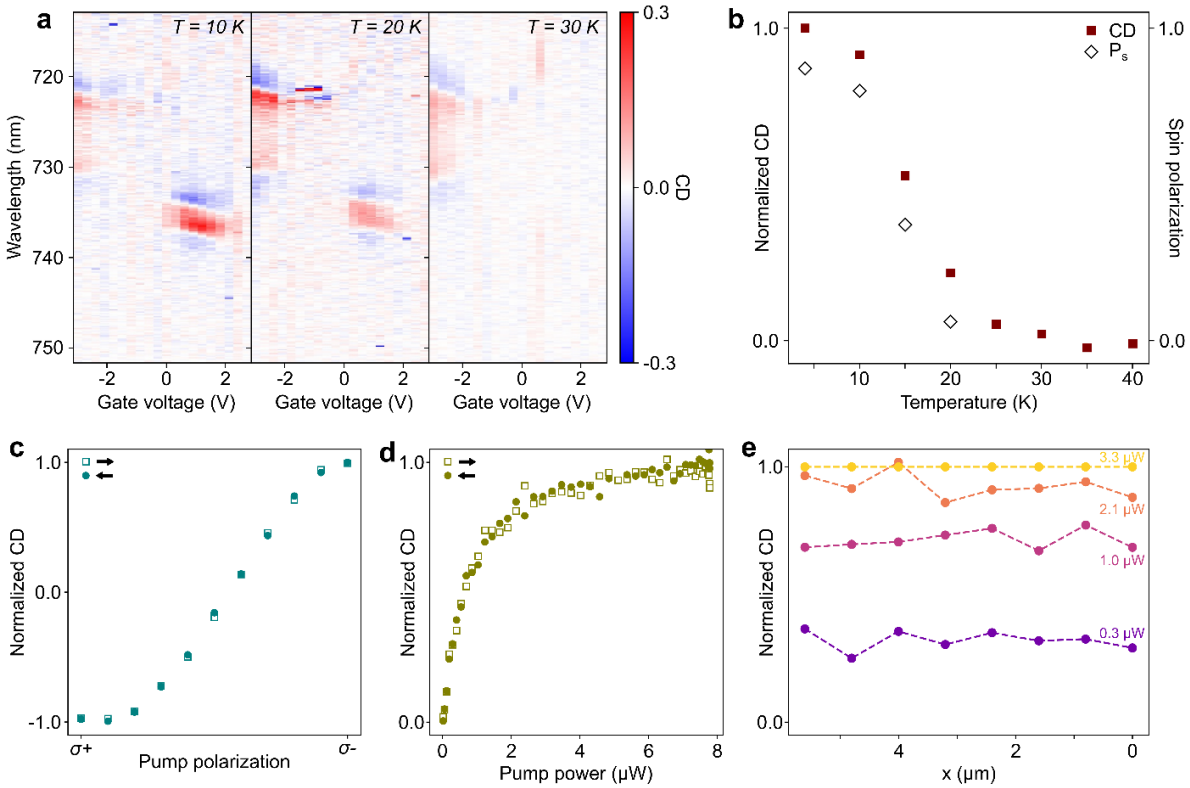

Figure 9: Stability of CD signal. a, Gate-dependent CD spectra of sample D2 at 10 K, 20 K and 30 K (pump-probe offset of 2.2 μm, pump power of 10 μW). b, Temperature dependence of triplet CD amplitude (red squares) selected from gate-dependent CD spectra at gate voltage of 1.2 V. Corresponding spin polarizations (hollow diamond) are extracted from reflection spectra. c, Polarization dependence of singlet CD amplitude of sample D1 (pump-probe offset of 1.6 μm, pump power of 7.8 μW). Hollow squares (solid circles) correspond to sweeping the polarization from σ+ to σ- (σ- to σ+). d, Power dependence of singlet CD amplitude of sample D1 (pump-probe offset of 1.6 μm). Hollow squares (solid circles) correspond to increasing (decreasing) pump power. e, Spatial dependence of singlet CD amplitude of sample D1 under selected pump powers, normalized to

heterostructure observed under microscope imaging, which correspond to observable dips in photoluminescence. The CD signal terminates upon crossing the noted defects.

To gain additional insight into the origin of the mesoscopic CD, we vary the doping concentration. As depicted in Figure 6c, we can access the intrinsic, hole-doped and highly electron-doped region by varying the gate voltage. Here, we study the long-range CD (i.e., pump-probe separation of 8 μm) within these different doping regions. As shown in Figure 6a, no CD signal is observed in the intrinsic region, implying the optically induced CD is correlated with free carriers in the system. As in Figure 8f, we observe strong CD co(cross)-polarized to the pump from the triplet (singlet) features. At higher doping concentrations, while the heavily-doped charged exciton X-- (Mahan exciton or attractive polaron) is clearly observed in reflectivity, there is no observable CD. We further characterize this by plotting the extracted peak amplitude (Fig. 8b) and CD amplitude (Fig. 8c) against the estimated doping density for different species of excitonic states. We observe that at 1.75 V, $n_c \approx 4 \times 10^{12}$ cm^{-2}, the system transitions from observable singlet and triplet trions with strong CD, to X-- exciton states with no

observable CD. Therefore, our measurements clearly correlate the CD with the singlet and triplet trion spectral features in the electron-doped regime. We also observe CD signal in the hole-doped region. We note that in the hole-doped regime, we are unable to fully quench the exciton reflectivity, indicating limited doping capability.

We also investigate the strength of the CD with respect to changes in temperature (on a second sample D2), pump polarization, and excitation power. Figure 9a depicts the doping dependent CD spectra at different temperatures. The CD signal vanishes at T = 30 K, even though reflection spectra still exhibit clear resonance features of singlet/triplet trions and X-- states (see Supplementary Information). The temperature dependent triplet CD amplitude and estimated spin polarization are plotted in Figure 9b, showing a rapid transition from an unpolarized (Ps = 0.06) to a polarized (Ps = 0.87) spin state as the temperature goes below T = 15 K. To gauge the impact of pump polarization on CD, we sweep the polarization from σ+ to linear and then σ- (Fig. 7c), observing the singlet CD signal increase from its minimum value through zero to its maximum value. When scanning in the opposite direction, the CD signal shows the same trend, vanishing at linear pump polarization. Lastly, we measure the impact of pump power on CD (Fig. 7d). The pump induces mesoscopic CD even with powers as low as 100 nW, and the CD signal begins saturating at ~2 μW. No hysteresis is observed when the pump power is scanned in the opposite direction, similar to the pump polarization scan. While the magnitude of the CD varies with pump power, the spatial profile of the CD remains nearly uniform within an order of magnitude variation in pumping power (Fig. 9e).

Analysis and impact: We attribute the mesoscopic spin polarization to ferromagnetic order in the TMDC induced by the optical pump. This claim is supported by the following observations: (I) In our measurements, mesoscopic spin-polarization emerges within the same carrier density regime as theoretically predicted and experimentally studied ferromagnetic phases in TMDCs. In theoretical models of electron-electron interactions in TMDCs, exchange inter- and intra-valley coupling lead to spin-polarized ferromagnetic phases at electron densities around $n_e \sim 10^{12}$ cm-2. These models were validated by experimental studies of magnetic phases in electron-doped monolayer molybdenum disulphide (MoS2) in an external magnetic field. In that case, strong exchange intervalley interactions – compared to the small spin-orbit splitting of the conduction bands in MoS2 – lead to band inversion and the spin polarization of resident electrons across both K and K' valleys (i.e., spin-polarized, but not valley-polarized electrons). In contrast, WSe_2 monolayers exhibit an order of magnitude larger spin-orbit splitting in the conduction band. Consequently, the predicted ferromagnetic ground state consists of spin/valley-polarized resident electrons, in agreement with our circular dichroism results. (II) The temperature dependence of the CD signal, which represents the magnetization, displays a trend qualitatively consistent with other 2D ferromagnetic materials, and criticality fits indicate a Curie temperature TC = 15 K with a critical exponent of 0.113, close to the value of 0.125 for a 2D Ising model. (III) The disappearance of spin polarization with increased electron doping signifies a 1st -order phase transition from a ferromagnetic to a paramagnetic phase. This is in full agreement with previous experimenta and theoretical studies of magnetic phase transitions in TMDs. (IV) We additionally observe signatures of long-range order in the hole-doped regime, consistent with theory, although yet to be shown experimentally.

A primary innovation in our study is the use of a continuous-wave optical pump to break the symmetry between equivalent magnetic phases and stabilize mesoscopic magnetic order against fluctuations. Magnetic state fluctuations explain both the absence of spin order below Tc without the optical pump and the lack of observable hysteresis in our time-averaged measurements. The fluctuations may arise due to nano-ampere-scale leakage currents in our sample, which can destabilize the magnetic state by injecting unpolarized electrons. The optical pump then stabilizes a single magnetic state against fluctuations by selectively valley-pumping spin-polarized electrons, thereby breaking the symmetry between degenerate magnetic states and preferentially favoring the formation of a co-polarized magnetic state. This mechanism is fundamentally different from previously reported all-optical control of magnetism, which is based on heating and inverse Faraday effects. We also emphasize that the optical pump should not be considered directly analogous to an external magnetic field as a symmetry breaking mechanism. In contrast to Zeeman interaction in a magnetic field, the optical pump does not change the energetics of the system. Additionally, the dynamics of the pump-induced spin polarization may lead to time-dependent evolution of the magnetic phase, which is not captured by our steady state measurements.

Critically, while the optical pump acts locally, the magnetic order is stabilized mesoscopically, extending well beyond the sub-micron pumping region to the boundaries of the monolayer. Our measurements afford some insight into the nature of this non-locality. We observe that, rather than spreading from the pump location in a non-linear fashion, the magnetism emerges uniformly over the sample with increasing pump power. This suggests that in the absence of optical pumping, long-range magnetic phases exist in the sample, but the phases fluctuate temporally between spin configurations. The optical pump acts to pin one of the two long-range magnetic phases against fluctuations. The micron-scale domain size in our measurements is comparable in size to magnetic domains in other 2D magnetic materials. This picture contrasts with a model in which the electronic ground state at zero applied magnetic field consists of local, nanoscale magnetic domains – in this picture, the pumping would not be expected to generate mesoscopic polarization beyond the locally controlled domains. Follow up studies will fully elucidate the dynamics of the magnetic phases and the process of long-range stabilization.

Further Elucidating Dynamics of Optically Controlled Magnetism:

In the previous sections, we explained how the optical resonances of the triplet and singlet trions could be used in order to probe the spin-polarization of WSe2. This has allowed us to optically explore the spin behavior of this material in equilibrium and dynamically. Our initial exploration of the dynamics found evidence that an injected spin-polarization grows as it propagates away from the source (spin-amplification). This finding prompted us to further investigate. In general, spin-polarization dynamics are determined by an amalgam of electronic structure, phonon, and electron-electron interaction factors which are difficult to fully untangle. To overcome this, we limit our scope to clear divergences from the predictions of a diffusive independent electron model. We have established that the spin-polarization dynamics are primarily driven by correlated phenomena rather than independent electron dynamics.

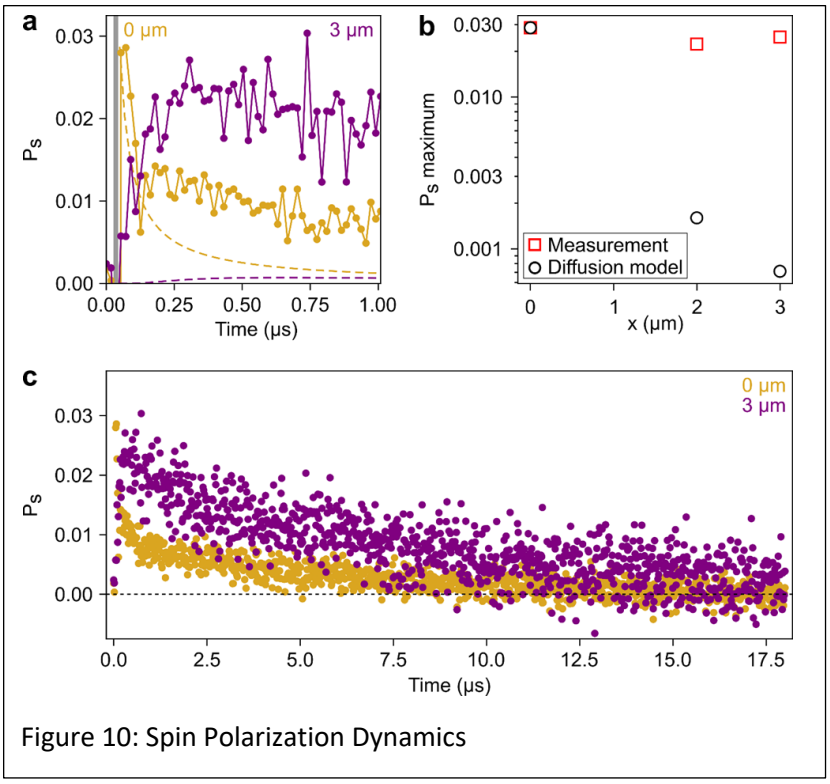

Figure 10: Spin Polarization Dynamics

There are two manifestations of correlated behavior in our system which are of practical interest for the primary research thrust. The first, spin-amplification, is of interest for our device and broadly to photonic computing systems because it can enable signal fan-out, or where a spin-polarization output signal from one device is able to reach multiple devices. The second is localization. We have observed that at sufficiently low doping regimes, the injected spin-polarization is local. However, a small change in doping can transition the spin polarization dynamics from the localized to amplifying regimes, with significant spin-polarization observed at distances larger than 11um. Control of the localization of spin-polarization signals can enable switchable crosstalk between devices on the same monolayer and opens the possibility of control schemes using electronic doping.

To understand this behavior, we performed extensive measurements of the temporal dynamics of the spin polarization with different pump/probe separations. We use a local, 5 ns pulsed laser at 633 nm to generate a spin imbalance under the pump and then measure spatially- and temporally-resolved changes to the spin polarization extracted from differential reflection. We observe that as the system evolves in time, mesoscopic spin polarization emerges at micron length scales over a microsecond timescale (Fig. 10a). The peak spin polarization observed exhibits no systematic change with increasing pump/probe separation (Fig. 10b, red squares), agreeing with the spatially uniform CD under CW pumping. The spin polarization at the pump location sets an upper bound for the optical spin polarization injection. After building up for hundreds of nanoseconds, the spin polarization detected away from the pump location exceeds that observed at the pump location. These results cannot be captured by a two-dimensional diffusion-decay model with pulsed excitation, which predicts at least an order of magnitude decay in polarization at three-micron separation regardless of the parameter estimates used for the carrier diffusion constant and relaxation time (see Supplementary Information). These results indicate that after the spin injection from the initial excitation pulse, the spin polarization is appreciably amplified across the sample and persists for over 10 μs (Fig. 10c).

Complementary to the amplification observed in the higher doping regimes is the localization of spin-polarization seen in the low doping regimes. Despite significant local spin-polarization,

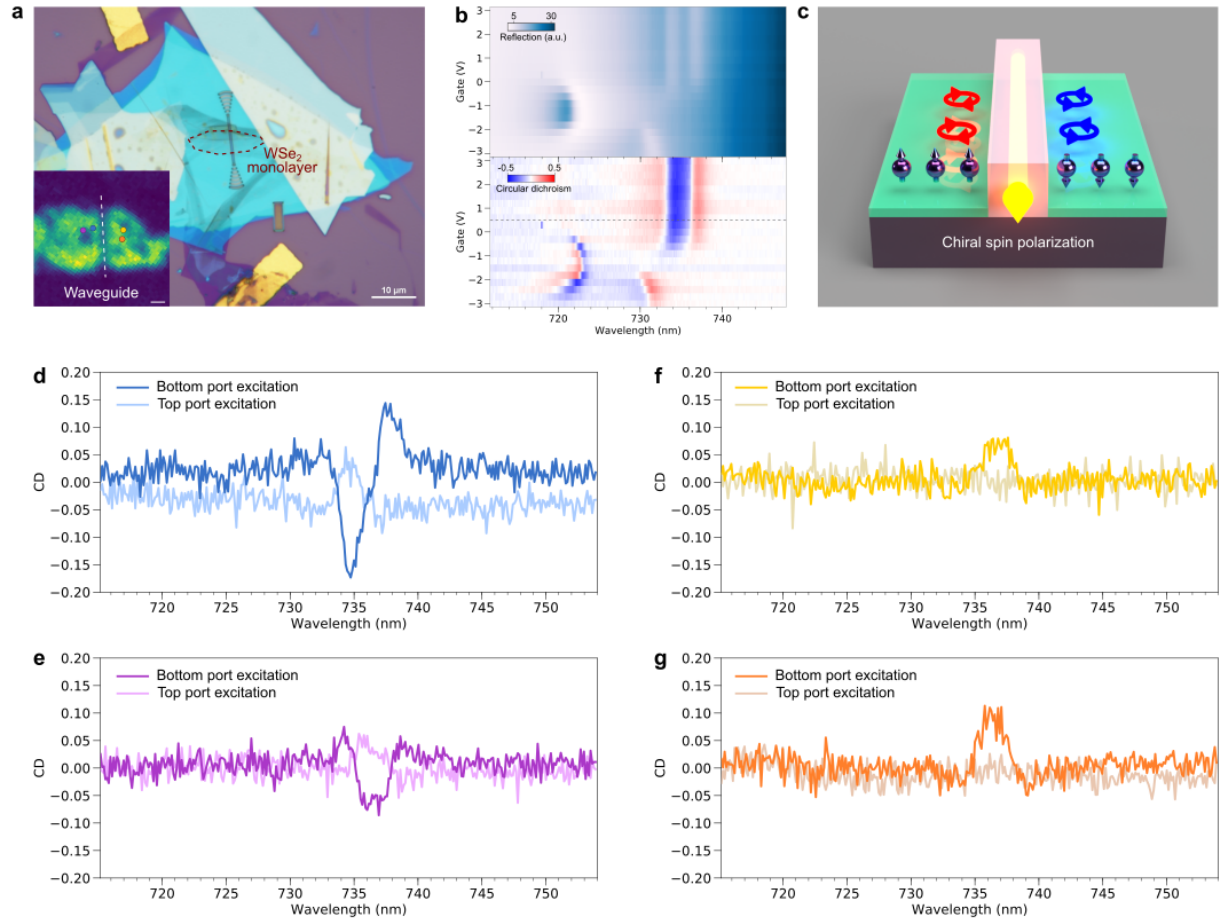

Figure 11: Control of magnetic order with waveguided optical pumps

supported both by the time dynamics and continuous wave data, non-local points exhibit zero spin-polarization at low doping. Fitting the local dynamics to an independent electron model then results in a similar divergence of measured versus observed dynamics.

These divergent phenomena, spin-amplification and spin-localization, are suggestive of dynamics driven primarily by strong electron-electron interactions rather than the typical independent electron dynamics. These are two manifestations of correlated behavior in our system that are of practical interest for device engineering. The first, spin-amplification, is of interest for our device and broadly to photonic computing systems because it can enable signal fan-out, or where a spin-polarization output signal from one device is able to reach multiple devices. The second is localization. Control of the localization of spin-polarization signals can enable switchable crosstalk between devices on the same monolayer and opens the possibility of control schemes using electronic doping. We will implement these collective phenomena in spin-opto-electronic devices in our future work.

(2) Control of magnetism with waveguided optical pumps

We also explored the direct control of solid-state memory, i.e. magnetism, with waveguided optical pumping. This can be utilized as an alternative mechanism to generating optical isolation, albeit with microwatt level control powers as opposed to milliwatt level control powers for optical Stark shift generated isolation. Additionally, the direct interface of a memory with light, in combination with analog element control, is highlighted as a critical need in photon-based neuromorphic computing. From a recent review in Nature Photonics: “Memory circuits that are able to interact directly with light can enable more agile reconfiguration in the processor.”

We developed a new fabrication method, shown in Figure 5, that will allow us to control the spin memory in the waveguide. To demonstrate the coupling between the nanophotonics and monolayer TMDs using the new fabrication method, we study spin polarization induced in the 2D material by optical pumping in the waveguide. We follow the same fabrication procedure outlined above, except now a WSe_2 monolayer is sandwiched between two BN flakes. The coupling is demonstrated by measuring the magnetic order on the two sides of the waveguide under different waveguide mode propagation direction.

The optical image of the device is shown if Figure 10a. Far field characterization of photoluminescence (inset of Figure 10a) and CD signal (Figure 10b) show that the encapsulated monolayer WSe2 still preserves it high quality, demonstrated by its bright photoluminescence and highly-tunable CD signal.

As illustrated by Figure 10c, the waveguide mode will drive the magnetic order oppositely on the two sides of the waveguide. We picked four points on the two sides of the waveguide (color points in inset of Figure 10a) and measured the CD signal at those points with pumping on the top (bottom) port. CD signal was measured to demonstrate the waveguided mode drive magnetic order on the two sides of the waveguide. The CD signal is summarized in Figure 10d. We can find that on the two sides of the waveguide, we have opposite magnetic order with the waveguide mode propagates in the same direction. When the propagating direction reversed, the sign of the CD signal also flips. Those results confirms that the waveguide efficiently couples to the monolayer WSe2 and successfully drives the magnetic order.